Direct determination of fluid-solid coexistence of square-well fluids confined in narrow cylindrical hard pores

Huan Cong Huang, Wen Wen Chen, Jayant K. Singh, Sang Kyu Kwak, et al.

View Online   Export Citation

ARTICLES YOU MAY BE INTERESTED IN

Vapor-liquid critical and interfacial properties of square-well fluids in slit pores
The Journal of Chemical Physics **130**, 214707 (2009); https://doi.org/10.1063/1.3148884

Characterization of fluid-solid phase transition of hard-sphere fluids in cylindrical pore via molecular dynamics simulation
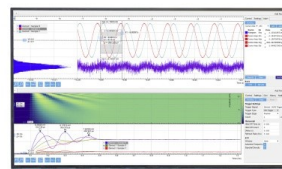The Journal of Chemical Physics **130**, 164511 (2009); https://doi.org/10.1063/1.3120486

Thin-thick surface phase coexistence and boundary tension of the square-well fluid on a weak attractive surface
The Journal of Chemical Physics **128**, 044708 (2008); https://doi.org/10.1063/1.2824503

Direct determination of fluid-solid coexistence of square-well fluids confined in narrow cylindrical hard pores

Huan Cong Huang,[1] Wen Wen Chen,[1] Jayant K. Singh,[2] and Sang Kyu Kwak[1,a)]

[1]*Division of Chemical and Biomolecular Engineering, School of Chemical and Biomedical Engineering, Nanyang Technological University, Singapore 637459*
[2]*Department of Chemical Engineering, Indian Institute of Technology Kanpur, Kanpur 208016, India*

Fluid-solid phase transition and coexistence of square-well fluids confined in narrow cylindrical hard pores are characterized using molecular simulation methods. The equation of state containing a fluid phase, a solid phase and a fluid-solid coexistence state was separately obtained for different attractive ranges of potential well and pore diameters; $\lambda=1.2$, 1.3, 1.4, and 1.5 for a pore of diameter $D=2.2\sigma$, $\lambda=1.5$ and 1.65 for a pore of diameter $D=2.5\sigma$. For $\lambda=1.2$, 1.3, and 1.4 at pore diameter $D=2.2\sigma$, $\lambda=1.5$ at $D=2.5\sigma$, the fluid-solid phase coexistence densities and pressure are close to the hard sphere fluids at the same temperature, while the pressure decreases significantly for $\lambda=1.5$ at $D=2.2\sigma$ and $\lambda=1.65$ at $D=2.5\sigma$, respectively. We also report the structural properties of the systems undergoing a phase transition. © *2010 American Institute of Physics*. [doi:10.1063/1.3429741]

I. INTRODUCTION

The square-well (SW) interaction potential plays an important role in the study of fluids as it is the simplest model containing both attractive and hard-core repulsive interactions. The thermophysical and structural properties of this model have been studied for many years in both theory and computer simulation due to practical similarities. Many results are available for vapor-liquid phase behaviors for the SW model.[1–4] There are several techniques to determine the vapor-liquid coexistence, such as Gibbs ensemble Monte Carlo (GEMC),[5] Gibbs–Duhem integration (GDI),[6,7] grand-canonical transition-matrix Monte Carlo,[2,8] but less is known about the fluid-solid behavior. Pagan and Gunton[9] used the free energy calculation and GDI to determine the fluid-solid coexistence and the metastable fluid-fluid coexistence for a short range SW model. Later, Liu *et al.*[10] combined GEMC with aggregation-volume-biased method in conjunction with GDI to develop the full vapor-solid, vapor-liquid, and liquid-solid phase diagrams of the SW model. The aforementioned studies indicate that the phase behavior of colloidal particles depends sensitively on the range of interaction, as has been known since the work of Gast *et al.*[11] So far, the studies of the fluid-solid coexistence have mainly focused on the bulk systems as shown previously.

On the other hand within some confinements,[12–14] the fluid-solid properties may exhibit significant deviation from the bulk ones due to geometrical size effects and the interaction of particles with confining walls. Our previous study[15] indicates a strong dependence of the fluid-solid coexistence of hard sphere fluids on the pore size and it is expected that both the range of interaction and pore size have significant effects to the fluid-solid behavior. Another important factor in studying the behavior of model fluids is the structure.

Several studies have investigated the ordering of particles under cylindrical confinement.[16–20] The structure of the confined fluids is highly dependent on the pore diameter and it seems there is no simple and continuous dependence, which can be generalized. Here we especially focus on the narrow pores, which can only hold one cylindrical layer of particles, and those are of great theoretical and experimental interest, as in such systems the particles can be self-assembled to form single helical or twisted helical structure. The systems resemble the colloids confined in very narrow channels for constructing nanowires,[21–23] peapod-related system such as C_{60} encapsulated in Carbon-nanotube,[19,24] and even the double helices of DNA on the large molecular scale.[25] Also, better and more understanding of the fluid-solid behavior and structure of these systems ultimately help to find practical nanoapplications in capillarity, lubrication, gas purification and storage, fabrication of nanofluidic devices, and provide important insights on the self-assembly helical structure, which is commonly found in the nature.

To this end, we elucidate the fluid-solid behavior and structure of the SW fluids under narrow cylindrical confinement using molecular simulation and modeling methods to investigate the effect of range of interaction and narrow pore sizes. The pore sizes are chosen to hold only one cylindrical shell of particles in such systems, which have small interface and fraction of particles due to small cross section. The free energy gap during the fluid-solid transition is small enough to ensure the equilibrium of the coexisting phases in the same simulation box, thus this makes a direct simulation of equilibrium of fluid and solid phases in one simulation box possible. The reset of this paper is organized as follows. In the next section, we briefly describe our systems and methods used for obtaining the equation of state and methods to characterize the structure of the confined SW fluids. Section

---

a)Author to whom correspondence should be addressed. Electronic mail: skkwak@ntu.edu.sg.

III describes the details of simulation conditions in this work. Section IV presents the results and discussion followed by the conclusion in Sec. V.

II. METHODOLOGY

We consider the system of SW particles confined in narrow cylindrical hard pore of diameter D. The particles are first arranged in cylindrical shell of triangular or square shape for $D=2.2\sigma$ and 2.5σ, respectively, where σ is the diameter of the confined particles. To obtain the accurate equation of state along an isotherm from fluid to solid including the coexistence regime, we have run series of molecular dynamics (MD) simulations. Once the equation of state is known, the fluid isotherm is fitted to a convenient fitting function of the form[26]

$$\beta P = \frac{\rho}{1-a\rho} + b\left(\frac{\rho}{1-a\rho}\right)^2 + c\left(\frac{\rho}{1-a\rho}\right)^3, \quad (1)$$

where ρ is the number density and $\beta=1/kT$ is the inverse temperature, where T and k are the temperature and the Boltzmann constant, respectively. The solid isotherm is fitted to a second order polynomial equation in the form of $\beta P = a+b\rho+c\rho^2$. The pressure values within the coexistence regime are averaged; the pressure at which both phases are in equilibrium, then the freezing and melting densities are obtained by solving the equation of state for both phases at this pressure. We separately performed the isobaric-isothermal Monte Carlo (NPT MC) simulations and compared the results to those of MD. The comparison indicates that MD is more efficient to evaluate the phase coexistence in such systems.

In this work, the pressure components of the SW fluid confined in the cylindrical pore using MD is obtained by using the virial theorem of the pairwise-additive potential,[27]

$$P_{\alpha\beta} = \rho kT + \frac{1}{V}\left\langle \sum_{i=1}^{N-1} \sum_{j>i}^{N} (r_{ij})_\alpha (f_{ij})_\beta \right\rangle, \quad (2)$$

where N is the number of molecules, r_{ij} is the relative position vector between the center of mass of molecules i and j, and $f_{ij}=-\nabla u_{ij}$ is the force between them at the potential energy u_{ij}. The angle bracket indicates the time average of MD or the ensemble average of MC. In the SW model, the collision of two particles occurs when the distance of two particles equal to hard-core. The forces between two particles, during the collision, have an infinite magnitude but act for an infinitesimal time. Each pair collision contributes an amount to the average of Eq. (2) when integrated over time, while the particle-wall collision has no contribution to the spreading pressure,

$$P_{\alpha\beta} = \rho kT + \frac{1}{V t_{\text{sim}}} \sum_{\text{collision}} (r_{ij})_\alpha (\Delta p_{ij})_\beta, \quad (3)$$

where t_{sim} is the total simulation time and the sum is over all collision occurring during this period, Δp_{ij} is the difference of momentum before and after the collision between atom i and j.

The microstructure of the system is monitored by the one-body radial density profile $\rho(r)$, the axial pair distribution function $g(z)$, bond order parameters Q_6 and two-dimensional (2D) hexagonal order parameter Φ_6. Of these three functions, the first two are used to monitor the radial and axial distribution of particles, respectively, and Q_6 and Φ_6 are used to monitor the global order of the system. The reduced radial density profile $\rho^*(r)$ is obtained by dividing the cylindrical pore into n concentric cylindrical shells with the same thickness then sample the number of particles divided by the shell volume. Thus, the definition of $\rho^*(r)$ can be expressed as

$$\rho^*(r_i) = \frac{\langle N_i \rangle}{\pi(r_i^2 - r_{i-1}^2)L}\sigma^3, \quad (4)$$

where N_i is the number of particles, whose distance to the pore axes are in the range of r_{i-1} to r_i, with $r_i=\Delta r \times i$, and Δr the thickness of the cylindrical shell. L is the length of the cylindrical pore. The axial pair distribution function $g(z^*)$ is modified from the pair correlation function, which is extracted from the following equation:

$$\int_{z^*=0}^{z^*=\infty} \rho^* g(z^*) \pi R^{*2} dz^* \approx N, \quad (5)$$

where N is the total number of particles, $\rho^*=\rho\sigma^3$ is the reduced density, $z^*=z/\sigma$ is the reduced axial distance, and $R^* =R/\sigma$ is the reduced pore radius. The upper limit of z^* is changed to the axial length of the simulation box, L/σ in calculation. The global order of the system indicates whether a system is fluidlike or solidlike and is characterized by the bond order parameters introduced by Steinhardt *et al.*[28] To calculate bond order parameters, we start from the spherical harmonic associated with every bond r_{ij} in the system. Here a bond is not chemical bond but a vector joining two neighboring atoms, whose distance is less than a cut off radius. The quantity is defined as[29]

$$Q_{lm} = Y_{lm}(\theta(r_{ij}), \phi(r_{ij})), \quad (6)$$

where Y_{lm} is the spherical harmonic and θ and ϕ are polar and azimuthal angles of the bond with respect to a fixed coordinate frame, which can be arbitrarily chosen. The global bond order parameter Q_l, which is rotationally invariant, is then defined as follows:

$$Q_l \equiv \left(\frac{4\pi}{2l+1} \sum_{m=-l}^{l} |\bar{Q}_{lm}|^2\right)^{1/2}, \quad (7)$$

where $\bar{Q}_{lm}$ is the average of Q_{lm}'s over all bonds in the system. In this study, we use Q_6, of which $l=6$ as the order parameter. Q_6 is very sensitive to the global structure, which significantly increases when the ordered structure appears and vanishes for the isotropic fluid. In addition to the bond order parameter Q_6 which captures the order of a system in three dimensions, we have also utilized the 2D order parameter Φ_6 defined as

$$\Phi_6 = \left| \frac{1}{M} \sum_{i=1}^{M} \frac{1}{N_i} \sum_{j=1}^{N_i} \exp(i6\theta_{ij}) \right|, \tag{8}$$

where M is the number of particles in the same cylindrical layer, N_i is the number of nearest neighbors of particles i. We define the nearest neighbors as those particles j within a distance 1.3σ from particles i, and θ_{ij} is the angle between two neighboring particles i and j and an arbitrary but fixed axis. The cylindrical layer is unrolled into a flat plane so that the 2D order parameter can be obtained. The value of Φ_6 equals to 1 for a perfect hexagonal plane, but far from 1 for a disordered phase.

III. SIMULATION MODEL AND DETAILS

In this work, the fluid-fluid interaction is represented by the SW potential,

$$u_{f-f} = \begin{cases} \infty, & 0 < r_{ij} < \sigma, \\ -\varepsilon, & \sigma \le r_{ij} < \lambda\sigma, \\ 0, & \lambda\sigma \le r_{ij}, \end{cases} \tag{9}$$

where $\lambda\sigma$ is the potential-well diameter, and ε is the depth of the energy well. The cylindrical pore is represented by the one body potential,

$$u_{w-f} = \begin{cases} \infty, & r < \sigma/2.0, \\ 0, & r \ge \sigma/2.0, \end{cases} \tag{10}$$

where r is the distance from the center of particle to the wall. In MD simulation, the wall acts as perfect rigid cylindrical surface. During the simulation, normal component of the momentum of the particle colliding with the wall is reversed while keeping the same magnitude. The periodic boundary condition is applied along the pore axis, which is chosen as z direction. We adopt the values of the units such that σ and ε are unity. All length scales are in unit of σ and other reduced units used in the work are the temperature $T^* = kT/\varepsilon$, pressure $P^* = P\sigma^3/\varepsilon$, and time $t^* = t/[\sigma(m/\varepsilon)^{0.5}]$. Note that the superscript asterisk will be omitted in the text below for the sake of convenience.

The MD simulations are first performed in canonical ensemble (NVT), i.e., during the simulation, the number of particle, the volume of simulation box, and the temperature are kept constant. The temperature was kept constant by simple momentum scaling, with all momenta multiplied by an appropriate factor at the end of each time step Δt so that the total kinetic energy of the system remains constant. The time step, Δt, was fixed at 0.05. The only effect of the time step is to determine the frequency of updating the properties measured in the simulation and rescaling the momenta to the desired temperature. The equilibrium period was set to follow two steps. We first set the simulation at $T = 10.0$ to ensure the particles are fully distributed in the cylindrical pore. Then the system was quenched to the target temperature. The total time steps for these two steps were set to 5×10^4 and we switched the simulation to microcanonical ensemble (NVE) to collect the equilibrium data. The time step for production was taken as 2×10^5 and we repeated each simulation five times. Longer simulations were performed for the coexist-

ence regime. The simulations were conducted with the system size of 1000 particles and we carefully checked that the system size is sufficient to avoid finite-size effect in our system. For the NPT MC simulations, the change in volume was made by changing the length of the cylinder keeping the diameter fixed. We performed N trials of displacing a randomly chosen particle followed by one trial of changing the pore length. The initial configuration was set to the random configuration at $\rho = 0.7$. For NPT simulations, equilibrium and production cycles were set to 5×10^5 in most cases.

IV. RESULTS AND DISCUSSION

In Fig. 1 we compare the equation of state of the SW fluid confined in a cylindrical pore of $D = 2.2$ obtained by MD and NPT MC. The MD simulations were first performed to obtain the pressure as the function of density. The values of pressure were then used as the input for the NPT MC simulations. Both results show good agreements on the fluid and solid branches. The discontinuity on the equation of state, which is observed from both methods, is indicative of the fluid-solid transition. This comparison indicates that both methods are accurate enough to determine the equation of state at both fluid and solid branches. However, for determining the fluid-solid coexistence regime, we find that MD is better than NPT MC, as MD not only has much smaller relaxation time, which enables us accurately to determine the coexistence density regime and coexistence pressure, while NPT MC generally cannot pinpoint these properties in such accuracy.

Figure 2 presents the equation of state of the SW fluid confined in the pore of $D = 2.2$ for $\lambda = 1.5$ at different temperatures. The result of hard sphere is plotted for a comparison as the infinite temperature limit ($\beta \to 0$), where the square well potential is reduced to hard sphere one. We can observe that for all temperatures studied, βP_{zz}'s are lower than that of hard sphere over the densities of interest, which indicates that the attractive forces actually affect the system
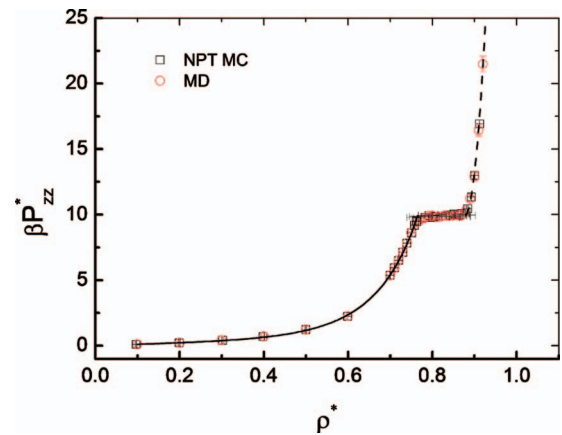

FIG. 1. Comparison of the equation of state (βP_{zz} vs ρ) of the SW molecules of $\lambda = 1.5$ confined in cylindrical hard pore of $D = 2.2$ at $T = 1.0$ obtained by NPT MC and MD simulations, which are represented by square and circle symbols, respectively. The solid line indicates the fit of result at fluid branch using Eq. (1), and the dash line is the second order polynomial fit to the solid branch. Error bars are the standard deviation of 5 independent runs.
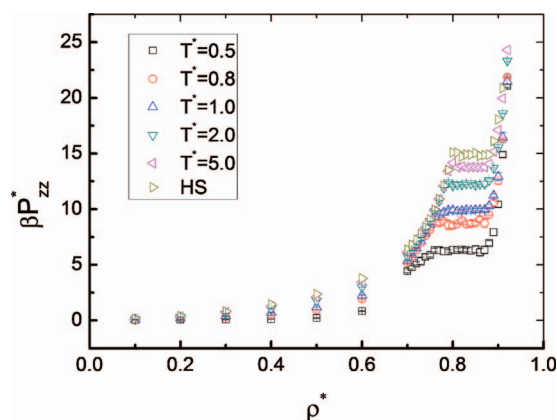
FIG. 2. The equation of state (βP_{zz} vs ρ) of the SW molecules of $\lambda = 1.5$ confined in a cylindrical hard pore of $D = 2.2$ at different temperatures 0.5, 0.8, 1.0, 2.0, and 5.0. The result of hard spheres confined in the same pore size is shown for comparison.

FIG. 4. The temperature-density fluid-solid phase diagram of the SW molecules confined in a cylindrical hard pore of $D = 2.2$ for the short range $\lambda = 1.2$ and the long range $\lambda = 1.5$, using MD simulation described in the text.

to be freezing at lower pressures. The equation of state at high temperature is always above that of low temperature including the fluid-solid coexistence branch. The coexistence spreading pressure becomes lower as the temperature reduces, which is also same for the fluid branch, and the coexistence range becomes larger as the temperature decreases due to the early start of the freezing at low temperature. Note that the relative differences in the coexistence spreading pressures would be dramatically larger if β is excluded from the figure, thus the effect of the temperature is considered to be large on the coexistence spreading pressure for $\lambda = 1.5$. Nevertheless, we found that the melting densities are almost invariant over the variation of the temperature.

With the same conditions of the system, the range of the interaction is decreased and Fig. 3 presents the results of $\lambda = 1.2$, 1.3, and 1.4 for $D = 2.2$. For a shorter attractive range $\lambda = 1.2$, the equation of state at high temperature is apparently above that of low temperature at the fluid branch, however, at $\rho > 0.7$, the differences of the equations of states at different temperatures vanish and those are observed to coincide at the solid and fluid-solid coexistence branch. Note that if β is omitted from Fig. 3, the reduced coexisting pressures show some differences, but not as dramatic as in the case of the
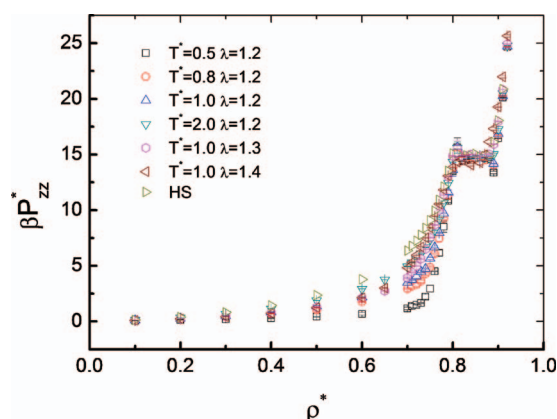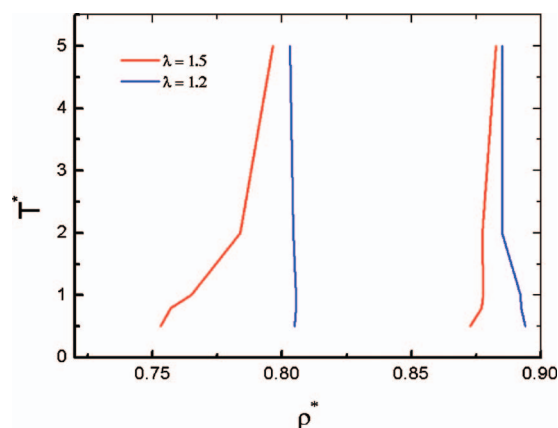
longer interaction range $\lambda = 1.5$ in this pore size. Consequently, freezing and melting densities change little with the temperature at this short attractive range, which is shown from Fig. 4. The equations of states for $\lambda = 1.3$ and 1.4 show the similar behavior of $\lambda = 1.2$, yet the fluid pressure slightly increases as λ increases from 1.2 to 1.4 at the same density, while the fluid-solid coexistence branch and solid branch are insensitive to the well extent.

With a slight increase of the pore size, the structure of the system is significantly changed from at most three coplanar molecules in $D = 2.2$ to four coplanar molecules in $D = 2.5$. Figure 5 shows the equation of state for the pore diameter $D = 2.5$. We found that, all equations of states of $\lambda = 1.5$ in $D = 2.5$ at different temperatures are close to each other to that of hard sphere except at the coexistence branch (i.e., slightly higher than that of hard sphere) while the case of $\lambda = 1.5$ in $D = 2.2$ shows large deviations of the equations of states at different temperatures. When the attractive range is increased to $\lambda = 1.65$ in $D = 2.5$, the behavior of the equation of state becomes similar to the case of $\lambda = 1.5$ in $D = 2.2$. It is shown that there exist some scale-up effect between the pore size and the interaction range in behavior of
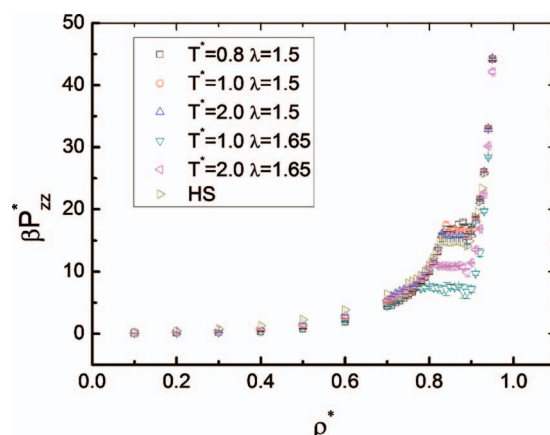

FIG. 3. The equation of state (βP_{zz} vs ρ) of the SW molecules of $\lambda = 1.2$ confined cylindrical hard pore of $D = 2.2$ at different temperatures 0.5, 0.8, 1.0, and 2.0, and $\lambda = 1.3$ and 1.4 at $T = 1.0$. The result of hard sphere is shown for comparison.

FIG. 5. The same equation of state as in Fig. 3 for $D = 2.5$ and $\lambda = 1.5$ at $T = 0.8$, 1.0, and 2.0, $\lambda = 1.65$ at $T = 1.0$ and 2.0. The equation of state of hard spheres confined in $D = 2.5$ is shown for comparison.

TABLE I. Fluid-solid coexistence data estimated from MD simulation of SW molecules confined in cylindrical pore with various well diameters under narrow pore sizes. The subscripts f and s represent fluid and solid, respectively. The number(s) in parentheses represent the error in the last digit(s).

	T	ρ_f	ρ_s	P_{zz}
		$D=2.2$		
$\lambda=1.2$	0.5	0.8049(3)	0.8941(3)	7.27(4)
	0.8	0.8053(2)	0.8924(3)	11.69(4)
	1.0	0.8053(4)	0.8922(4)	14.69(8)
	2.0	0.8042(4)	0.885(1)	29.5(1)
	5.0	0.803(1)	0.885(1)	74.2(6)
$\lambda=1.3$	1.0	0.7991(4)	0.8837(4)	14.93(7)
$\lambda=1.4$	1.0	0.799(2)	0.867(1)	14.4(2)
$\lambda=1.5$	0.5	0.753(2)	0.872(2)	3.14(3)
	0.8	0.757(3)	0.877(1)	7.01(13)
	1.0	0.765(1)	0.877(1)	9.90(4)
	2.0	0.784(2)	0.877(1)	24.4(3)
	5.0	0.7964(3)	0.882(1)	68.8(1)
HS[a]	1.0	0.803(1)	0.878(2)	14.91(9)
		$D=2.5$		
$\lambda=1.5$	0.8	0.836(2)	0.906(1)	13.69(35)
	1.0	0.836(1)	0.905(1)	16.56(20)
	2.0	0.8347(7)	0.9016(8)	31.13(15)
$\lambda=1.65$	1.0	0.756(5)	0.9045(4)	7.33(29)
	2.0	0.803(1)	0.9019(2)	21.77(10)
HS[a]	1.0	0.826(2)	0.893(3)	14.8(4)

[a]Reference 15.

the equation of state even with the variation of the structure (i.e., triangular to square shape, see Fig. 10). The detailed coexistence properties are listed in Table I.

Figure 6 shows the bond order parameter Q_6 as the function of density in the pore size $D=2.2$. Q_6 in the current work is found to be nonzero for dilute fluid due to a confinement effect. The system with a random set of bonds has a Q_l value of $1/\sqrt{N_b}$ but not zero[30] as within the tight confinement, the direction of bonds joining each pair of atoms is not stochastic but has limited orientations. An interesting phenomenon has been observed with the increase of the density
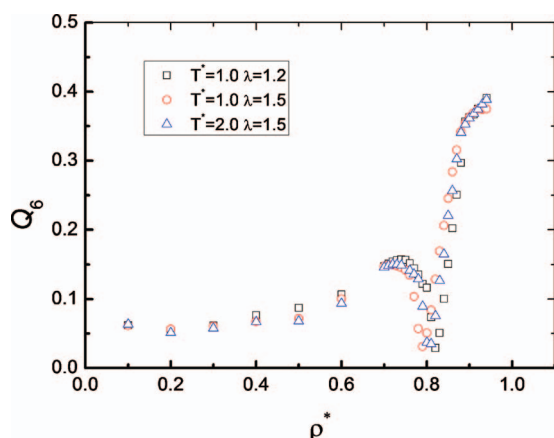

FIG. 6. The bond order parameter Q_6 as the function of density for the SW molecules confined in a cylindrical hard pore of $D=2.2$ at different temperature and potential range. Symbols square, circle and triangle represent system at $T=1.0$ and $\lambda=1.2$, $T=1.0$ and $\lambda=1.5$, $T=2.0$ and $\lambda=1.5$, respectively.
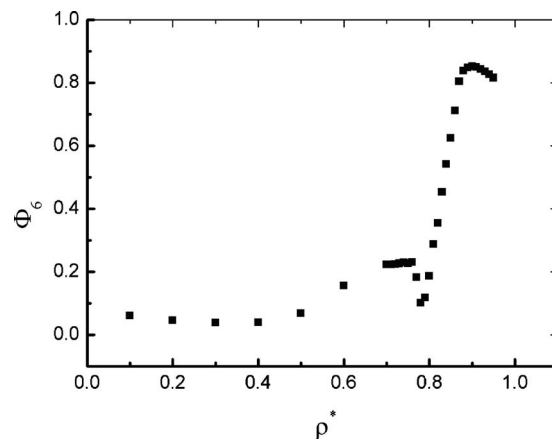

FIG. 7. The 2D bond order parameter Φ_6 as the function of density for the SW molecules confined in a cylindrical hard pore of $D=2.2$ at $T=1.0$ and the potential range $\lambda=1.2$.

of the fluid. Q_6 increases to reach a value around 0.15 at the density around 0.75. Similar behavior is found for Φ_6 with slight increase within this density range, as shown in Fig. 7. However, the equation of state shows that the system is still in fluid phase at this density. Since the particles form a structure of spiral tetrahedra along the pore axis, an ordered structure is created even for the fluid phase under a narrow confinement. With further increase of the density, Q_6 and Φ_6 decrease to a minimal value and increase sharply. Over this density range, the phase transition can be associated with the structure of spiral packing of tetrahedra transforming to tri-
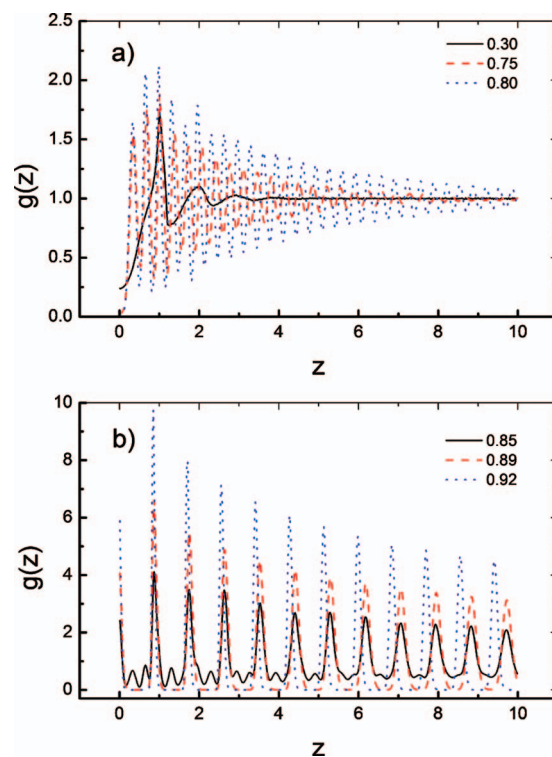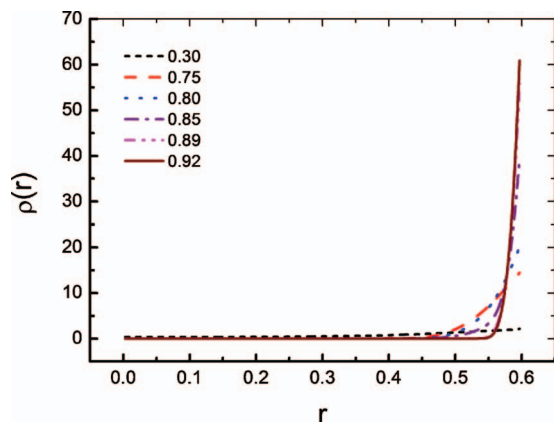

FIG. 8. Axial pair distribution function $g(z)$ for the SW molecules confined in cylindrical pore of $D=2.2$ at $T=1.0$ and $\lambda=1.2$, at different average densities, 0.30 (dilute fluid), 0.75 (dense fluid), 0.80 (around freezing density), 0.85 (within fluid-solid coexistence), 0.89 (around melting density), and 0.92 (solid).

FIG. 9. Radial density profiles $\rho(r)$ for the same system as in Fig. 8.

angular packing of three particles rotated with an angle of $\pi/3$ against the nearest layer of the triangular particles along the pore axis (see Fig. 10).

To understand the structure in details, the axial distribution function $g(z)$ and the density profile $\rho(r)$ are studied, as shown in Figs. 8 and 9. Also, the snapshots of all systems of
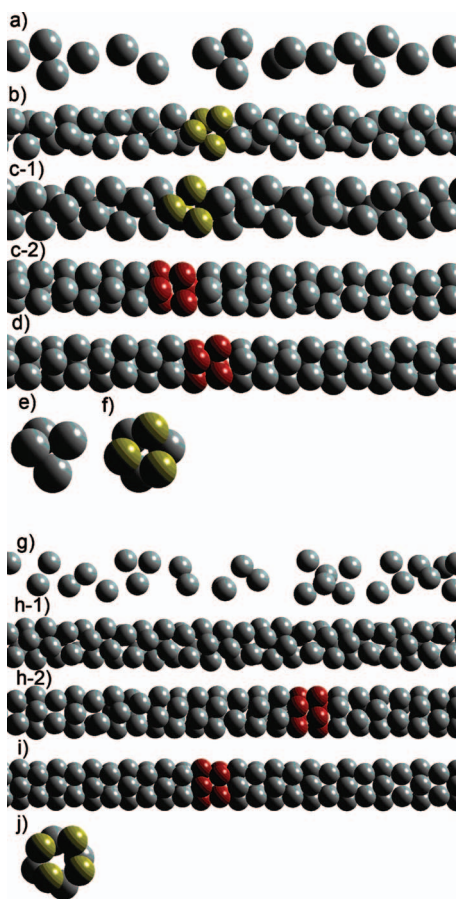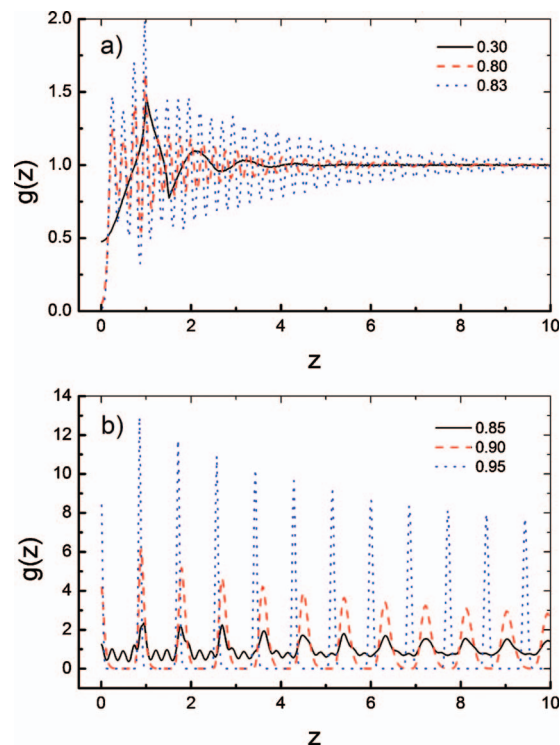

FIG. 11. Axial pair distribution function $g(z)$ for the SW molecules confined in cylindrical pore of $D=2.5$ at $T=1.0$ and $\lambda=1.5$, at different average densities, 0.30 (dilute fluid), 0.80 (dense fluid), 0.83 (around freezing density), 0.85 (within fluid-solid coexistence), 0.90 (around melting density), and 0.95 (solid).

interest are presented in Fig. 10 for convenient view. At the density 0.3, $g(z)$ shows a peak at $z=1.0$ and a valley at $z=1.2$, which happen to be the hard core diameter and the potential well extent, respectively and it quickly decays to 1.0 as z increases, thus the system does not have a long range order at this density. For $\rho=0.75$ and 0.80, two peaks appear at $z<1.0$, followed by the peaks periodically appeared at the interval of about 0.33, and the value of $g(z)$ at $z=0$ is nearly zero. The two bond order parameters suggest that there is a partial ordered phase of spiral packing of tetrahedra appears around this density range. Indeed, the position of peaks at $g(z)$ matches with the axial distance of the peaks of the tetrahedron. For density 0.85 (within coexistence), 0.89 (around melting point), and 0.92 (solid phase), a sharp peak appears at $z=0$, and the peak at $z=1.0$ moves to $z\approx0.87$, followed by series of peaks periodically appeared at the interval about 0.87. This phenomenon indicates that the tetrahedral packing thus is transformed to triangular packing. Note that for the density within coexistence, there exist two small peaks between the sharp peak at $z=0$ and $z\approx0.87$, which indicates that both tetrahedral and triangular packings are coexisting in the system. There is no distinct discontinuity in $\rho(r)$ as density increases, however, $\rho(r)$'s vary near to the wall at low densities, which indicates that the particles are loosely packed and even makes the pocket of particles at the lowest density of interest. This behavior is attributed to the entropic dominance on the system, that particles spontaneously move to the more accessible space to maximize the entropy of the system. In the narrow pore, which can hold only one layer of particles at a plane perpendicular to the z direction, the at-

FIG. 10. Snapshots for the SW molecules confined in the narrow cylindrical pores of $D=2.2$ (*a* to *d*), and $D=2.5$ (*g* to *i*) at different average densities: *a*, $\rho=0.3$ (dilute fluid), *b*, $\rho=0.75$ (dense fluid, spiral packing of tetrahedron), *c*, $\rho=0.85$ (fluid-solid coexistence), *d*, $\rho=0.92$ (solid, triangular packing), *g*, $\rho=0.3$ (dilute fluid), *h*, $\rho=0.85$ (fluid-solid coexistence) and *i*, $\rho=0.95$ (solid, square packing). The tetrahedral, triangular, and square packings are shown in *e*, *f*, and *j*, respectively. Two different structures are found in the corresponding coexistence densities in $D=2.2$ (*c*-1 and *c*-2) and $D=2.5$ (*h*-1 and *h*-2).

tractive force has little impact to the radial density profile and the behavior of $\rho(r)$ is similar to that of hard sphere systems confined in hard pores discussed by Duran-Olivencia *et al.*[16] Similar behavior was also observed in D =2.5, as seen in the $g(z)$ function shown in Fig. 11, where three peaks are observed at $z<1.0$ at $\rho=0.80$, 0.83, and 0.85 indicating a twisted helical structure, and disappear at $\rho=0.90$ and 0.95, where the structure is transformed to a square shape consisting of four particles sharing the same z against another nearest square layer by rotating an angle of $\pi/4$.

V. CONCLUSION

In this work, we have studied the phase behavior of the SW fluid confined in narrow cylindrical pore using molecular simulation methods. The full equation of state including a fluid phase, a solid phase and a fluid-solid coexistence was calculated for a wide range of temperature and various attractive ranges for the pore diameter $D=2.2$ and 2.5. Based on our experience in the work and the comparison with NPT MC simulation, we consider the MD method to be a good choice to determine the equation of state, especially for the fluid-solid coexistence. We found that there is a threshold of the attractive range λ, below which the fluid-solid behavior varies little with respect to temperature and close to that of hard spheres under same thermodynamic condition. In addition to the fluid-solid coexistence calculation, we also present the structure properties of the system from dilute fluid to solid. In particular, we found a partially ordered structure in the dense fluid due to the strong confining effect of the boundary; the mix of triangle and square shapes of the SW particles was observed.

We note that our characterization of the fluid-solid phase transition is based on observing the distinct constant pressure in the equation of state (i.e., P_{zz} versus ρ^*) under constant temperature. In bulk, the constant pressure region (i.e., fluid-solid phase transition) is unobtainable for the hard sphere system by using the generic NVT MD simulation, however, the same method has shown its capability to capture the emergence of the phase transition for the hard sphere fluid confined in the cylindrical pore without any extra recipe in simulation technique.[15] In this study, although the occurrence of the phase transition has been assessed even with coinciding variation of calculated order parameters, we alert that one must not think of this particular phase transition as the first-order transition without a proof of thermodynamic phase equilibria. The absence of the driving force of the phase equilibria or the discontinuity of the free energy. Unfortunately, the development for the free energy calculation in-

volving cylindrical pore has been little or none to our knowledge. It is rare even for the hard sphere but currently initiated with a free volume approach by our group, thus a full investigation on the first-order transition of the system of interest is to be done in future work.

[1] J. K. Singh, D. A. Kofke, and J. R. Errington, J. Chem. Phys. **119**, 3405 (2003).
[2] J. K. Singh and S. K. Kwak, J. Chem. Phys. **126**, 024702 (2007).
[3] H. L. Vörtler and W. R. Smith, J. Chem. Phys. **112**, 5168 (2000).
[4] J. K. Singh, G. Sarma, and S. K. Kwak, J. Chem. Phys. **128**, 044708 (2008).
[5] A. Z. Panagiotopoulos, Mol. Phys. **61**, 813 (1987).
[6] D. A. Kofke, Mol. Phys. **78**, 1331 (1993).
[7] D. A. Kofke, J. Chem. Phys. **98**, 4149 (1993).
[8] J. R. Errington, J. Chem. Phys. **118**, 9915 (2003).
[9] D. L. Pagan and J. D. Gunton, J. Chem. Phys. **122**, 184515 (2005).
[10] H. Liu, S. Garde, and S. Kumar, J. Chem. Phys. **123**, 174505 (2005).
[11] A. P. Gast, C. K. Hall, and W. B. Russel, J. Colloid Interface Sci. **96**, 251 (1983).
[12] L. D. Gelb, K. E. Gubbins, R. Radhakrishnan, and M. Sliwinska-Bartkowiak, Rep. Prog. Phys. **62**, 1573 (1999).
[13] H. K. Christenson, J. Phys.: Condens. Matter **13**, R95 (2001).
[14] F. R. Hung, B. Coasne, E. E. Santiso, K. E. Gubbins, F. R. Siperstein, and M. Sliwinska-Bartkowiak, J. Chem. Phys. **122**, 144706 (2005).
[15] H. C. Huang, S. K. Kwak, and J. K. Singh, J. Chem. Phys. **130**, 164511 (2009).
[16] F. J. Durán-Olivencia and M. C. Gordillo, Phys. Rev. E **79**, 061111 (2009).
[17] G. T. Pickett, M. Gross, and H. Okuyama, Phys. Rev. Lett. **85**, 3652 (2000).
[18] M. C. Gordillo, B. M. Haya, and J. M. Romero-Enrique, J. Chem. Phys. **125**, 144702 (2006).
[19] M. Hodak and L. A. Girifalco, Phys. Rev. B **67**, 075419 (2003).
[20] K. Koga and H. Tanaka, J. Chem. Phys. **122**, 104711 (2005).
[21] Y. Yin and Y. Xia, J. Am. Chem. Soc. **125**, 2048 (2003).
[22] S. A. Vanapalli, C. R. Iacovella, K. E. Sung, D. Mukhija, J. M. Millunchick, M. A. Burns, S. C. Glotzer, and M. J. Solomon, Langmuir **24**, 3661 (2008).
[23] K. E. Sung, S. A. Vanapalli, D. Mukhija, H. A. McKay, J. M. Millunchick, M. A. Burns, and M. J. Solomon, J. Am. Chem. Soc. **130**, 1335 (2008).
[24] L. A. Girifalco and M. Hodak, Appl. Phys. A: Mater. Sci. Process. **76**, 487 (2003).
[25] L. Stryer, *Biochemistry* (Freeman, New York, 1988).
[26] B. Barboy and W. M. Gelbart, J. Chem. Phys. **71**, 3053 (1979).
[27] M. P. Allen and D. J. Tildesley, *Computer Simulation of Liquids* (Clarendon, Oxford, 1987).
[28] P. J. Steinhardt, D. R. Nelson, and M. Ronchetti, Phys. Rev. B **28**, 784 (1983).
[29] P. M. Reis, R. A. Ingale, and M. D. Shattuck, Phys. Rev. Lett. **96**, 258001 (2006).
[30] M. D. Rintoul and S. Torquato, J. Chem. Phys. **105**, 9258 (1996).